JOURNAL OF MATERIALS SCIENCE **38** (2003) 1359– 1364

Grain boundary devitrification of Ca α-sialon ceramics and its relation with the fracture toughness

Y. ZHANG*,†, Y.-B. CHENG
School of Physics and Materials Engineering, Monash University, Victoria 3800, Australia
E-mail: yu.zhang@nist.gov

Grain boundary devitrification was carried out on three Ca α-sialon ceramics with different grain sizes and morphologies and various amounts of grain boundary glass. The devitrified product was gehlenite in all samples, indicating that the crystallization of the Ca oxynitride glass was accompanied by a volume reduction. The volume reduction upon crystallization and the thermal expansion mismatch between the devitrified product and α-sialon grains would result in tensile residual stresses located at multi-grain junctions. These residual tensile stresses were expected to promote the crack deflection and bridging mechanism and thus to improve the material toughness. However, indentation fracture toughness measurement and scanning electron microscope study showed that there was no significant difference in fracture toughness and the fracture mode in present samples prior to and post heat treatment. This may be attributed to a change in the chemistry of the residual glass as a result of the grain boundary devitrification, which could enhance the bonding strength between the adjacent α-sialon grains. The enhanced bonding strength could have to some degree hindered the crack deflection and bridging mechanism.

1. Introduction

Since Si and N have low solid-state diffusivities below the decomposition temperature of Si_3N_4, liquid-phase sintering is the most commonly used method for densifying silicon nitride based ceramics [1]. The by-product of such liquid-phase sintering is, upon cooling, a remnant oxynitride glass phase, which exists as an interconnected network through the major crystalline phases in the final product. Therefore, the properties of silicon nitride based ceramics are significantly influenced by the properties of the intergranular glass.

Engineering of the grain boundary phase can alter the bonding strength and the residual stress level in silicon nitride ceramics and thus allows tailoring of the mechanical properties of these materials. Early theoretical work by Pompe and Kessler [2] established the value of the average stress and its fluctuations in various phases of silicon nitride ceramics. They concluded that a combined adjustment of internal thermal expansion mismatch and crystallization of the grain boundary amorphous phase could improve the mechanical properties of these materials. Recent experimental work by Pezzotti and Kleebe [3] investigated the influence of residual stresses at multi-grain junctions on the fracture toughness of silicon nitride materials. They found that residual tensile stresses at multi-grain junctions induced by crystallization of grain boundary glass with a negative volume change promoted the intergranular crack propagation and hence improved the fracture toughness, while residual compressive stresses resulted in a high fraction of transgranular crack propagation and a low fracture toughness. Thus, by varying the nature of the microscopic stress fields in silicon nitride materials, the fracture mode and consequently the fracture toughness of these materials could be altered.

It has been long recognized that complete crystallization of the grain boundary amorphous phase cannot be achieved in silicon nitride based ceramics [4–7]. In addition, the crystallization process results in an outdiffusion of non-stoichiometric species to the residual glassy phase and thus alters the chemical composition of the residual glass [8, 9]. The chemistry of the intergranular glass has been found to have a large effect on the fracture toughness of silicon nitride based ceramics [10]. Therefore, in order to better understand the effect of grain boundary crystallization on fracture toughness of silicon nitride based ceramics, the combined role of residual stress and grain boundary chemistry needs to be considered.

In this study, three Ca α-sialon compositions containing various amounts of intergranular glassy phase were selected to study the effect of grain boundary

*Author to whom all correspondence should be addressed.
†Currently guest Scientist at National Institute of Standards and Technology, Gaithersburg, MD 20899-8500, USA.

crystallization on fracture toughness. The crystallization of the grain boundary glassy phase of these materials was achieved by post-sintering heat-treatment. The effects of grain boundary crystallization on fracture toughness were examined in terms of both residual stress and grain boundary chemistry.

2. Experiments

Compositions of Ca α-sialon can be represented by the formula $Ca_xSi_{12-(m+n)}Al_{(m+n)}O_nN_{16-n}$, where $x = m/2$, and m and n are substitution numbers referring to m(Al—N) and n(Al—O) bonds replacing $(m+n)$(Si—N) bonds in each unit cell [11]. The three Ca α-sialon samples selected for this work have an $m{:}n = 2{:}1$ ratio with the nominal x value of 0.5, 1.3 and 1.8, respectively. The designation CA1005 refers to a design composition of $m = 1.0$ and $n = 0.5$, and CA2613 and CA3618 describe the materials of compositions $m = 2.6, n = 1.3$ and $m = 3.6$, $n = 1.8$, respectively. Powders of Si_3N_4 (H. C. Starck, Goslar, Germany, Grade M11), AlN (H. C. Starck, Goslar, Germany, Grade AT) and $CaCO_3$ (APS Chemicals, NSW, Australia, Laboratory Grade) were ball milled in isopropanol for 30 h using Si_3N_4 milling balls. Subsequently the powders were dried in a fan-forced oven at 84°C. The weight percentages of the starting powders of the three compositions are shown in Table I. Approximately 8 g of powder was uniaxially pressed into 25 mm diameter pellets, followed by cold isostatic pressing at 200 MPa. The green pellets were first calcined at 900°C for 1 h in vacuum to decompose $CaCO_3$ to CaO. Sintering was carried out at 1800°C for 4 h in a graphite resistance heated furnace in nitrogen atmosphere. Furnace heating rates were 20°C min^{-1}. Cooling took place in the furnace by switching off the power after the scheduled dwell. Post-sintering heat treatment was carried out at 1300°C for 12 h in nitrogen.

The phases present in the Ca α-sialon ceramics were identified using X-ray diffraction (XRD) analysis, carried out on a Rigaku-Geigerflex diffractometer with nickel filtered CuK_α radiation. Microstructures of the polished and etched samples were examined using a JEOL FE6300 scanning electron microscope (SEM) equipped with a field emission gun. Etching was performed by immersing polished surfaces of the samples into molten NaOH (~400°C) for 10 s. Prior to SEM examination, the samples were carbon coated to prevent charge accumulation. The accelerating voltage used was 10 kV.

The diameter and length of the α-sialon grains were determined as the shortest and the longest dimensions, respectively, of the grains on the two-dimensional SEM micrographs of polished and etched surfaces. Over 500 grains of each sample were measured. The apparent aspect ratio of the grains was given by the ratio of the average length over average diameter. No stereological factors were considered here. The volume fraction of the minor AlN-polytypoids and intergranular glassy phase of α-sialon ceramics was estimated from the two-dimensional polished sections using quantitative image analysis technique. The SEM micrographs of the polished sections were enlarged and the area fraction of the minor AlN-polytypoids or intergranular glassy phase was manually traced on the transparent film for quantitative image analysis.

TABLE I Weight percentages of the starting powders of the three compositions

Composition	Si_3N_4 (wt%)	AlN (wt%)	CaO (wt%)
CA1005	84.602	10.590	4.808
CA2613	61.981	26.148	11.871
CA3618	48.964	35.105	15.931

The fracture toughness of the sialon ceramics was measured using the Vickers indentation method at a load of 98 N [12]. A value of 240 GPa for Young's Modulus was used to evaluate the fracture toughness of the Ca α-sialon materials [13]. The indentation toughness undervalues the actual toughness of these α-sialon ceramics in which an R-curve behaviour is expected [14]. However, such technique is adequate for a relative comparison of the resistance to the crack growth of ceramic materials. After the indentation measurements were made, the samples were slightly etched in molten NaOH at 400°C for 6 s and then carbon coated for SEM investigation of the crack propagation mechanism.

3. Results

XRD spectra for the as-sintered and heat-treated α-sialons are shown in Figs 1a and b, respectively. The crystalline phases present in these materials were identified using Powder diffraction files [15]. As can be seen, in as-sintered CA1005, α-sialon was the only crystalline phase revealed (Fig. 1a). In as-sintered CA2613, a trace of 33R phase was observed in addition to the dominant α-sialon phase (Fig. 1a). In as-sintered CA3618, a minor AlN′ phase presents along with the predominant α-sialon phase (Fig. 1a). The 33R and AlN′ phases are AlN defect structures resulting from the incorporation of silicon and oxygen atoms into the AlN structure [16, 17]. In heat-treated samples, XRD spectra revealed a secondary gehlenite phase ($Ca_2Al_2SiO_7$, G′) in samples CA2613 and CA3618 (Fig. 1b). Gehlenite is the crystallised form of the intergranular glass and the very low content of this phase (<3%, see below) in CA1005 indicates a very low amount of glass in the sample. The result is consistent with the fact that the CA1005 composition is located inside the single-phase α-sialon forming region.

SEM micrographs of polished and chemically etched surfaces of the three as-sintered Ca α-sialon ceramics are shown in Fig. 2. The differentiation of the phases present in the samples was made based on the XRD (Fig. 1a) and energy dispersive X-ray (EDX) (Fig. 2d) analyses. The average diameter and apparent aspect ratio of α-sialon grains as well as the volume fraction of the intergranular glass of these materials are given in Table II. Sample CA1005 contained more or less equiaxed α-sialon grains coupled with a small amount of intergranular glassy phase (Fig. 2a). The size of the α-sialon grains varied widely from 0.1 μm to over 2 μm with an average diameter of 0.44 μm. The volume fraction of the intergranular glassy phase in sample CA1005 was estimated using image analysis to be approximately 3%.

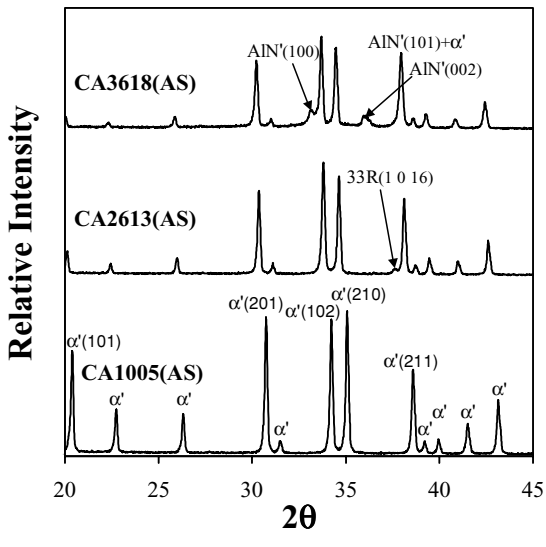

(a)

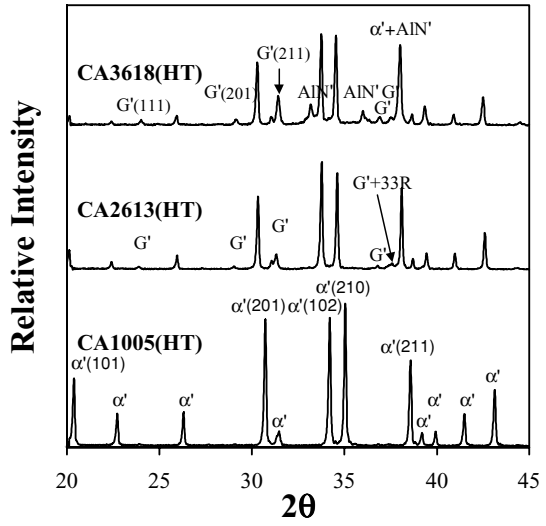

(b)

Figure 1 XRD spectra of Ca α-sialon samples: (a) as-sintered; and (b) heat-treated at 1300°C for 12 h. Note: $\alpha' = $ Ca α-sialon; $33R = SiAl_{10}O_2N_{10}$ (AlN-polytypoid); AlN′ = aluminium nitride solid solution (AlN-polytypoid); G′ = Gehlenite ($Ca_2Al_2SiO_7$) or more likely gehlenite solid solution ($Ca_2Al_{2-x}Si_{1+x}O_{7-x}N_x$ [18]).

Sample CA2613 displayed two distinct crystalline phases: the α-sialon phase with a smooth trait and the AlN-polytypoid phase with speckled features (Fig. 2b). XRD analysis suggested that the AlN-polytypoid phase in sample CA2613 was 33R. EDX analysis revealed that the grains with speckled feature consisted mainly of Al and N, indicating that they are the AlN-polytypoids (Fig. 2d). The speckled appearance of AlN-polytypoid was the result of the faster etching rate of AlN compared to that of α-sialon when NaOH etchant was used [19]. The α-sialon grains appeared mainly in an elongated shape and ranged widely in size. The small grains were typically 0.2–0.3 μm in diameter and 0.7–1.2 μm in length, while the large grains were 0.9–1.2 μm in diameter and 3–8 μm in length. Their aspect ratios were, however, very similar, ranging from 3 to 8 with an apparent ratio of 5.2. The 33R AlN-polytypoid appeared as long laths with an average thickness and length of 0.6 μm and 4 μm, respectively. Quantitative image analysis on the SEM micrographs of polished sections showed that the area fraction of 33R phase in sample CA2613 was approximately 4%, while the area fraction of the intergranular glassy phase in CA2613 was approximately 7%.

Sample CA3618 also consisted of two crystalline phases: the α-sialon and AlN′ phases (Fig. 2c). The α-sialon phase in CA3618 had a similar elongated grain morphology to that observed in material CA2613 except being much larger and longer in size. The average diameter of α-sialon grains in material CA3618 was 0.57 μm, although some grains were as large as 2 μm in diameter. The apparent aspect ratio was 7.3. The AlN′ phase, as shown with speckled features in Fig. 2c, exhibited a similar morphology as the 33R phase observed in CA2613. The size of these AlN′ grains was, however, much larger than that of the 33R laths in sample CA2613. Image analysis revealed that the area fraction of the AlN′ phase and the intergranular glassy phase in sample CA3618 was approximately 19% and 15%, respectively.

The measured room temperature fracture toughness of the three α-sialon materials before and after crystallization is presented in Table II. It can be seen that the fracture toughness increases with the grain diameter and apparent aspect ratio as well as the amount of the intergranular glassy material. A trend of a small increment in fracture toughness of heat-treated samples compared to their as-sintered counterparts is also observed, especially in materials containing larger and longer grains with higher amount of intergranular glassy phase. However, such increment is so small that it has the same magnitude as the measurement error.

TABLE II Properties of the three Ca α-sialon ceramics

Sample	Average diameter (μm)	Apparent aspect ratio	Intergranular glassy phase (vol%)	Toughness (MPa $m^{1/2}$)	
				As-sintered	Heat-treated
CA1005	0.44	1.8	3	4.5 ± 0.1	4.6 ± 0.4
CA2613	0.46	5.2	7	5.4 ± 0.5	5.5 ± 0.1
CA3618	0.57	7.3	15	5.7 ± 0.3	5.9 ± 0.2

4. Discussion

It is well established, both theoretically and experimentally, that the amorphous phase in silicon nitride based materials exists as intergranular thin films present at two-grain interfaces and as excess glass located at multi-grain junctions [4, 20, 21]. The intergranular films usually have a partially ordered structure with a typical equilibrium thickness of 0.5–2.0 nm depending on the composition of the materials [6, 8, 22]. Therefore, these thin films are energetically stable and cannot be further crystallized. Crystallization of the grain boundary amorphous phase mainly takes place at multi-grain junctions. However, high-resolution electron microscopy examination of devitrified silicon nitride ceramics showed that even at those multi-grain junctions, complete crystallization of the amorphous phase could not be achieved. A thin amorphous film remains between the crystalline grain boundary phases and the

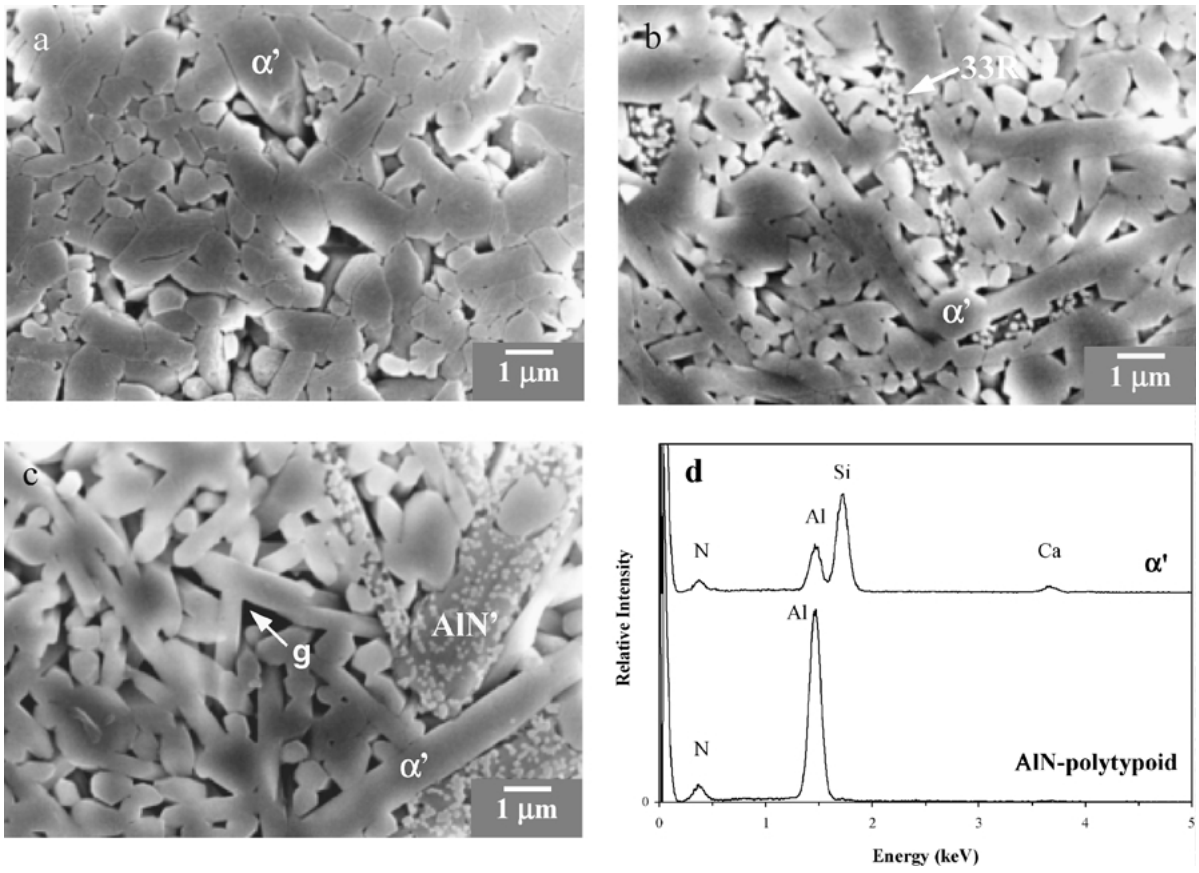

Figure 2 SEM micrographs of the as-sintered Ca α-sialon samples: (a) CA1005; (b) CA2613; and (c) CA3618. The samples were polished and chemically etched in molten NaOH for 10 s prior to SEM examination. EDX analysis (d) revealed that regions containing speckled particles, see Figs 2b and c, consisted mainly of Al and N, suggesting that they are probably precipitates of the AlN-polytypoid (33R and AlN′). Note: EDX spectrum for the Ca α-sialon phase (α') is also shown in (d) and g = intergranular glass.

silicon nitride grains [23]. There are two reasons for the existence of this film. First, the change in composition of the residual amorphous phase resulting from the crystallization process could have reduced the crystallization rate, and secondly, the volume reduction induced by crystallization process could have created tensile hydrostatic stress at the multi-grain junctions which hinders the further devitrification process [7].

In Ca α-sialon ceramics, the grain boundary glassy phase is oxynitride glass that contains calcium, because the solubility of Ca^{2+} cations into the α-sialon unit cell is limited [11, 24]. When CaO was used as the calcium source, previous quantitative measurement showed that the solubility of Ca^{2+} in α-sialon structure was approximately 70% of the nominal values for compositions ranging in $x = 0.3$–1.4, indicating that around 30% of Ca^{2+} remained in the grain boundary glassy phase [24]. More significantly, the above solubility level was found to continuously decrease as the nominal x value further increased [24].

In the present study, the post-sintering heat treatment of Ca α-sialons produces a crystalline gehlenite phase. However, devitrification of intergranular Ca oxynitride glass cannot be completed under the current heat-treatment condition (1300°C for 12 h). One possible reason is that the gehlenite phase observed in the Ca α-sialon system is a member of the melilite group and can exist as a solid solution incorporating a small amount of nitrogen with the general formula $Ca_2Al_{2-x}Si_{1+x}O_{7-x}N_x$ [18]. Therefore, the formation of the gehlenite solid solution consumes more oxygen than nitrogen and hence may result in a residual glass with increased nitrogen content. The increased nitrogen content increases the viscosity of the residual glass because in the structure of glass, nitrogen possesses three bonds to cations, which increases the packing density and the stiffness of the network [25]. This high viscosity residual glass requires higher temperature and longer time to crystallize due to the decrease of cation diffusivity and mobility. In fact, a previous study on the crystallization behaviour of bulk glasses in the Mg-Ca-Al-Si-O-N system showed that a complete crystallized glass-ceramic could not be prepared even after heat treatment at 1350°C for 20 h [26].

Another reason for the incomplete crystallization of the Ca oxynitride glass is the radial tensile stress resulting from the crystallization of the excess glass at the multi-grain junctions. Crystallization of the Ca-containing oxynitride glass is combined with a volume reduction due to the higher density of crystalline gehlenite phase. The volume change, of approximately 10 vol% [26, 27], leads to the generation of radial tensile stresses in the triple junctions at the interface between α-sialon and the gehlenite phase. In addition, the formation of the gehlenite phase can result in an internal stress at the interface between the gehlenite and α-sialon grains due to the thermal expansion mismatch. Because of the higher thermal expansion coefficient of

gehlenite relative to α-sialons [25], this thermal stress is also tensile in nature.

These tensile stresses resulting from both volume reduction and thermal expansion mismatch may be relaxed by two possible mechanisms: (1) viscous flow of the amorphous phase at two-grain interfaces into crystallizing multi-grain junctions; and (2) solution of primary grains into the amorphous film at two-grain interface, and diffusion into and reprecipitation at crystallizing multi-grain junctions [5]. Stress relaxation via viscous flow of the amorphous phase into crystallizing multi-grain junctions will result in a reduction of the intergranular film thickness. However, the viscous thinning of the amorphous film may not be kinetically favoured since the amorphous film is in equilibrium in the sense of an equilibrium thickness as proposed by Clarke [4]. This leaves solution-reprecipitation of the primary grains as the main stress relaxation mechanism. However, the annealing temperature of 1300°C is too low to cause a significant solution and reprecipitation of α-sialon. Thus tensile stresses persist at the annealing temperature and the strain energy associated with these stresses acts as a thermodynamic barrier which opposes the further devitrification process [2, 5].

As discussed above, crystallization of the grain boundary oxynitride glass can result in significant radial tensile stresses at the multi-grain edges in Ca α-sialon systems. It is therefore expected that any propagating crack tip is driven towards these multi-grain junctions and, as observed by Pezzotti and Kleebe, when such junctions are located near the acicular silicon nitride grains, elastic bridging can occur and thus result in an increased fracture toughness [3]. However, the elastic bridging effect and its associated improved fracture toughness are not as significant as one would expect in the present Ca α-sialon samples. Our results showed that though a tendency of improvement in fracture toughness after heat treatment exists, especially in materials containing coarser grains with higher apparent aspect ratio and larger amount of intergranular glass, the increment in fracture toughness is so small that it cannot be confidently determined by the indentation method.

SEM examinations of indentation cracks interacting with elongated Ca α-sialon grains in the heat-treated sample CA3618 revealed that, although the crack tip tended to propagate towards the multi-grain junctions, α-sialon grains were fractured both intergranularly (55%) and transgranularly (45%) (Fig. 3a). The ratio of the intergranularly fractured grains to transgranularly fractured grains is similar to that observed in as-sintered CA3618 material, suggesting that there is no significant increased incidence of elastic bridging in the heat-treated sample compared to the as-sintered sample. This may be attributed to the crystallization of "bulk" grain boundary oxynitride glass, which may lead to an enrichment of the nitrogen content in the intergranular glass film and the residual glass at the multi-grain junctions. The higher nitrogen content in the residual glass structure, as discussed earlier, could increase the packing density and the stiffness of the network and thus could increase the bonding strength between the α-sialon grains. The increased bonding strength at the two-grain interface could in turn hinder the crack deflection and bridging mechanism. Our high-resolution SEM examination of the crack tip vicinity revealed clear evidence of preferred motion of the crack tip towards the multi-grain junctions, however, in some cases, when the crack met the strongly bonded two-grain interfaces, transgranular fracture occured (Fig. 3b).

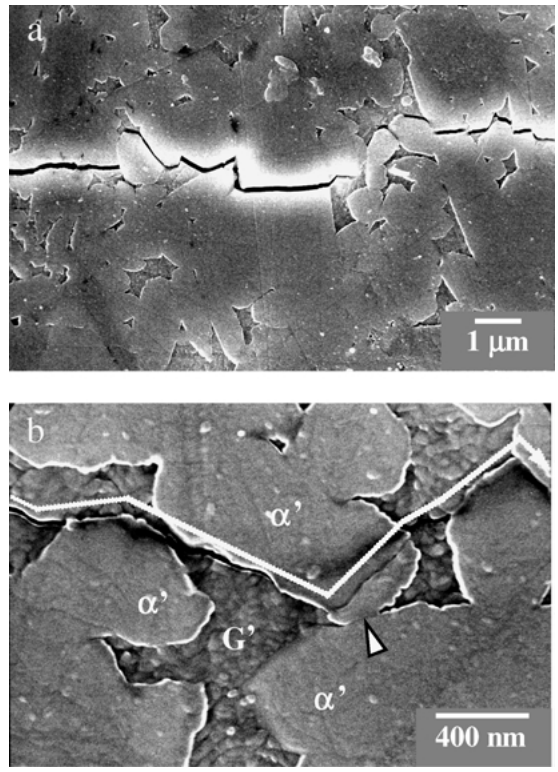

Figure 3 SEM observations of the interaction between a propagating crack and α-sialon grains of heat-treated sample CA3618: (a) a general view revealed that the fracture modes were both intergranular and transgranular; and (b) a higher magnification micrograph revealed when a propagating crack tip met the strongly bonded two-grain interface (indicated by arrow), in some cases, transgranular fracture occurred. Note: α' represents the α-sialon grains and G′ represents the grain boundary gehlenite phase.

Based on the experimental observations from the present study and from the previous work by Pezzotti and Kleebe [3], the following model may be proposed to describe the effect of devitrification on the fracture toughness of silicon nitride based materials.

In most silicon nitride based ceramics, an appropriate post-sintering heat treatment produces secondary crystalline phases at the multi-grain junctions. The volume reduction resulting from crystallisation of the amorphous phase and the thermal stress induced from the thermal expansion mismatch between the primary and the devitrified phases could produce radial tensile stresses at the multi-grain junctions. The radial tensile stresses tend to drive the propagating crack tip towards the multi-grain junctions. However, depending on the secondary phases formed, the chemistry of the residual glass, in the two-grain interfaces and the multi-grain junctions, may be altered, which could change the bonding strength between the grains. A weakened

bonding strength between the two-grain interface could promote crack bridging toughening mechanism and thus significantly increase the fracture toughness, while a strengthened bonding strength may hinder the crack deflection and bridging mechanism.

5. Conclusions

This work has examined the possible effects of the crystallization of intergranular glass on the fracture toughness of Ca α-sialon ceramics. The following conclusions can be made from the results of this study:

- Crystallization of the intergranular glass could introduce residual tensile stresses at the multi-grain junctions of Ca α-sialon ceramics.
- Crystallization of the intergranular glass may change the chemical composition of the residual glass of these materials.
- The effect of the grain boundary devitrification on the fracture toughness of these materials is based on the combined role of residual stress and grain boundary chemistry.

Acknowledgements

The authors are grateful to Prof. Michael J. Hoffmann for his encouragement and many critical comments on the manuscript.

References

1. F. L. RILEY, *J. Am. Ceram. Soc.* **83**(2) (2000) 245.
2. W. POMPE and H. KESSLER, in "Tailoring of Mechanical Properties of Si_3N_4 Ceramics," edited by M. J. Hoffmann and G. Petzow, NATO ASI Series, Series E: Applied Science, vol. 276 (Kluwer Academic Publishers, Dordrecht, The Netherlands, 1994) p. 353.
3. G. PEZZOTTI and H.-J. KLEEBE, *J. Eu. Ceram. Soc.* **19** (1999) 451.
4. D. R. CLARKE, *J. Am. Ceram. Soc.* **70**(1) (1987) 15.
5. H. KESSLER, H.-J. KLEEBE, R. W. CANNON and W. POMPE, *Acta metall. Mater.* **40**(9) (1992) 2233.
6. H.-J. KLEEBE, M. J. HOFFMANN and M. RUHLE, *Z. Metallkd.* **83**(8) (1992) 610.
7. G. BERNARD-GRANGER, J. CRAMPON and R. DUCLOS, *J. Mater. Sci. Lett.* **14** (1995) 1362.
8. M. J. HOFFMANN, in "Tailoring of Mechanical Properties of Si_3N_4 Ceramics," edited by M. J. Hoffmann and G. Petzow, NATO ASI Series, Series E: Applied Science, vol. 276 (Kluwer Academic Publishers, Dordrecht, The Netherlands, 1994) p. 233.
9. H.-J. KLEEBE, M. K. CINIBULK, I. TANAKA, J. BRULEY, J. S. VETRANO and M. RUHLE, in "Tailoring of Mechanical Properties of Si_3N_4 Ceramics," edited by M. J. Hoffmann and G. Petzow, NATO ASI Series, Series E: Applied Science, vol. 276 (Kluwer Academic Publishers, Dordrecht, The Netherlands, 1994) p. 259.
10. H.-J. KLEEBE, G. PEZZOTTI and G. ZIEGLER, *J. Am. Ceram. Soc.* **82**(7) (1999) 1857.
11. G. Z. CAO and R. METSELAAR, *Chem. Mater.* **3** (1991) 242.
12. G. R. ANTIS, P. CHANTIKUL, B. R. LAWN and D. B. MARSHALL, *J. Am. Ceram. Soc.* **64**(9) (1981) 533.
13. W. TA, Y.-B. CHENG, B. MUDDLE, C. HEWETT and M. TRIGG, *Mater. Sci. Forum* **325** (2000) 199.
14. C. A. WOOD, H. ZHAO and Y.-B. CHENG, *J. Am. Ceram. Soc.* **82**(2) (1999) 421.
15. Powder diffraction files JCPDS-ICDD: 42-0252 (α-sialon, $m = 1.36$, $n = 0.68$); 42-0164 (33R); 25-1133 (AlN); 35-0755 (Gehlenite).
16. G. VAN TENDELOO, K. T. FABER and G. THOMAS, *J. Mater. Sci.* **18** (1993) 525.
17. H. ZHAO, S. P. SWENSER and Y.-B. CHENG, *J. Eu. Ceram. Soc.* **18** (1997) 1053.
18. J. W. T. VAN RUTTEN, H. T. HINTZEN and R. METSELAAR, *J. Eu. Ceram. Soc.* **16** (1996) 995.
19. A. W. WEIME, Carbide, Nitride and Boride Materials Synthesis and Processing (Chapman & Hall, London, 1997) p. 159.
20. D. R. CLARKE, T. M. SHAW, A. P. PHILIPSE and R. G. HORN, *J. Am. Ceram. Soc.* **76**(5) (1993) 1201.
21. D. R. CLARKE and G. THOMAS, *ibid.* **60**(11–12) (1977) 491.
22. I. TANAKA, H.-J. KLEEBE, M. K. CINIBULK, J. BRULEY, D. R. CLARKE and M. RUHLE, *ibid.* **77**(4) (1994) 911.
23. J. S. VETRANO, H.-J. KLEEBE, E. HAMPP, M. J. HOFFMANN and R. M. CANNON, *J. Mater. Sci. Lett.* **11** (1992) 1249.
24. P. L. WANG, C. ZHANG, W. Y. SUN and D. S. YAN, *J. Eu. Ceram. Soc.* **19** (1999) 553.
25. S. HAMPSHIRE, E. NESTOR, R. FLYNN, J.-L. BESSON, T. ROUXEL, H. LEMERCIER, P. GOURSAT, M. SEBAI, D. P. THOMPSON and K. LIDDELL, *ibid.* **14** (1994) 261.
26. M. DECKWERTH and C. RUSSEL, *J. Non-Cryst. Solids* **217** (1997) 55.
27. *Idem.*, *ibid.* **217** (1997) 66.

Received 26 April 2001
and accepted 5 November 2002